

Efficient removal of Pb(II), Hg(II) and As(III) ions by a recyclable low cost magnetic hydroxyapatite nanocomposite from aqueous solution

Shaimaa T. El-Wakeel

Water Pollution Research Department, Environmental Research Division, National Research Centre, 33 EL Bohouth St., Dokki, Giza 12622, Egypt, Tel. +202 33371211; Fax: +202 33370931; emails: shaimaa_tw@yahoo.com/shaimaa.tw@gmail.com

Received 6 May 2021; Accepted 4 August 2021

ABSTRACT

In this study iron waste from the steel industry and eggshells biomass were used to prepare the environmentally-friendly magnetic hydroxyapatite composite. The prepared composite was characterized and applied for Pb(II), Hg(II) and As(III) removal from aqueous solution. Batch experiments show the adsorption capacity to be 348.3, 291.4 and 266.2 mg/g for Pb(II), Hg(II) and As(III) respectively, by applying the different isotherm models and the second-order kinetic model described well the adsorption process. Metals regeneration and the reuse of the prepared composite up to four cycles were obtained. The results revealed that the prepared composite synthesized from egg-shell and iron waste could be an effective and economically viable adsorbent for Pb(II), Hg(II) and As(III) ions.

Keywords: Heavy metals; Magnetite nanoparticles; Hydroxyapatite; Adsorption; Lead; Mercury; Arsenic

1. Introduction

Heavy metal ions are one of the toxic pollutants that accumulate and laying for several years in the living [1] and their released directly or indirectly into the environment as a result of rapid industrialization have created a major concern [2].

The existence of toxic metals such as Hg(II), Pb(II) and As(III) in water and wastewater causes severe health effects such as muscles weakness, stomach and chest pain and many carcinogenic effects [1,3,4]. An upper limit for lead has been set to be 50 and 15 µg/L by the World Health Organization (WHO) and the Environmental Protection Agency (EPA), respectively [5].

Although mercury (Hg) ions exist in low concentrations, its ability for accumulation makes it is always a challenge in water treatment [6,7]. Arsenic occurs in both inorganic and organic forms in natural waters and is classified as

one of the most toxic and carcinogenic chemical elements and can be found in two oxidation states, arsenate As(V) or arsenite As(III). As(III) is known to be 60 times more toxic than As(V) due to its higher mobility, [8] and the World Health Organization (WHO) has set the maximum limit of arsenic in potable water to be 10 µg/L.

Among the different methods adopted for heavy metals removal, Adsorption is the preferred method due to its simplicity, high efficiency, easy of handling and cost-effectiveness [9].

New studies tend to use low-cost, non-toxic and environmentally friendly adsorbents such as biomass like eggshells and agricultural by-products like nutshells for heavy metals removal [10,11]. Hydroxyapatite nanoparticles are a biocompatible material that is widely used as a biomaterial in medicine and used for heavy metals adsorption and can be prepared using bio-products like natural gypsum and eggshells [12].

Magnetite nanoparticles are used also extensively for metals adsorption due to the large surface area and high efficiency of separation by an external magnetic field [13,14].

Iron oxide and hydroxyapatite composites provide a promising method to prepare adsorbents that have large sorption capacities and easy recovery via magnetic separation [15].

The present study considers the preparation of magnetite nanoparticles from iron waste then compositing the prepared magnetic particles with hydroxyapatite produced from eggshells using the chemical precipitation method. The preparation process reduces the environmental impacts of these wastes producing a magnetic recoverable composite.

The prepared magnetic hydroxyapatite nanoparticles were applied for Pb(II), Hg(II) and As(III) removal from aqueous solution under different operating conditions.

2. Materials and methods

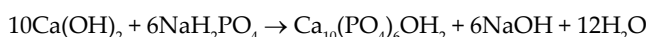
2.1. Materials

Chemicals of $\text{Pb}(\text{NO}_3)_2$, HgCl_2 , NaAsO_2 , NaBH_4 and ammonia solution were of analytical grade and used without further purification.

2.2. Methods

2.2.1. Synthesis of hydroxyapatite from eggshell HA

Eggshells were collected and cleaned by boiling water then calcined in air at 900°C for 1 h (heating rate of $10^\circ\text{C}/\text{min}$). The calcined powder was grounded. The organic matter was decomposed in the calcination step and calcium carbonate was converted into calcium oxide (CaO). $\text{Ca}(\text{OH})_2$ is formed after mixing the obtained CaO with distilled water, then it mixed with NaH_2PO_4 and the pH value was kept at 10 using 1 M ammonia solution. In general, solutions were mixed to obtain a Ca/P molar ratio of 1.66. The final solution was dried and calcined at 400°C for 1 h ($10^\circ\text{C}/\text{min}$ heating rate), then hydroxyapatite (HA) crystalline powder was obtained according to the following equation:



2.2.2. Preparation of magnetic nanoparticles from steel industry waste

Iron-containing waste samples were crushed and sieved to a fine powder then digested with concentrated HCl for 5–6 h. The concentration of Fe(III) in the digested sample was determined using the standard analytical procedure. The concentration of Fe(III) in a known volume of the digested solution was reduced to metallic iron by the addition of NaBH_4 solution. The formed metallic iron was separated out by filtration and dissolved in a known amount of Fe(III) to form Fe(II) solution then the Fe(II) concentration was estimated. Finally, magnetite nanoparticles were obtained by precipitating Fe(III) and Fe(II) solutions through the addition of ammonia solution.

2.2.3. Preparation of magnetic hydroxyapatite nanoparticles

The prepared HA obtained after calcination is added to Fe(III) solution by a mass ratio 1:1 of total Fe:HA, then

magnetite precipitation occurred by the addition of Fe(II) solutions at pH10–12 by ammonia solution.

2.3. Characterization techniques

The structure of the prepared magnetic hydroxyapatite nanocomposite (MHAP) and HA were characterized by powder X-ray diffraction spectrometry (XRD) using Bruker D8 ADVANCE (Bruker, Germany) instrument between 5° and 80° (2θ) at a scanning rate of $4^\circ/\text{min}$. The surface morphology of the prepared MHAP and HA were determined by a high-resolution transmission electron microscope (HR-TEM, JEOL 2100, Japan) at 200 kV after sonication and field-emission scanning electron microscopy using (FE-SEM; JEOL 6400 F, USA) with energy-dispersive X-ray spectrometry (EDX) operating at 5 kV.

Magnetic properties were measured in the solid-state using a vibrating sample magnetometer. The saturation magnetization value was determined from the plateau region of the magnetic flux density of a solid sample at 8000. The functional groups of the prepared adsorbents were identified by Fourier-transform infrared spectrometry (FTIR) analysis using FTIR-6100 (JASCO, Japan) instrument via the KBr pressed disc method, in a range from 400 to $4,000\text{ cm}^{-1}$ wavenumbers. The Brunauer–Emmett–Teller surface area was determined by N_2 adsorption and desorption measurements at 77 K using BELSORP MAX (BEL Japan Inc.). Fe(II) concentrations were measured by UV-Visible double beam spectrophotometer (JASCO V630, Japan) at 235 nm. Total iron and other metals concentrations were determined by inductively coupled plasma optical emission spectrometry (ICP-OES) (Agilent 5100, USA) in the prepared samples.

2.4. Adsorption studies

The adsorption behavior of the prepared MHAP for metal ions (Pb(II), Hg(II) and As(III)) was investigated by batch removal experiments at room temperature. Stock solutions of the metal ions were prepared using $\text{Pb}(\text{NO}_3)_2 \cdot 6\text{H}_2\text{O}$, HgCl_2 and NaAsO_2 salts dissolved in deionized water. Freshly prepared working metals solutions of concentrations 10 mg/L by diluting stock solutions with deionized water were used in the experiments. The samples were collected at different time intervals and filtered with a $0.45\ \mu\text{m}$ syringe filter membrane. The pH effect on the adsorption was studied by adjusting the solution pH with sodium hydroxide (NaOH) and nitric acid (HNO_3). The effect of the adsorbent dose was studied by changing the dose from 0.05–2 g/L. All adsorption tests were performed in triplicate.

The removal efficiency and the adsorbed amount were calculated using the following equations:

$$\text{Metals Removed}(\%) = \frac{C_0 - C_e}{C_0} \times 100 \quad (1)$$

The experimental data obtained in batch studies were used to calculate the adsorption capacity q_e (mg/g) at equilibrium using the following equation,

$$q_e = (C_0 - C_e) \frac{V}{m} \quad (2)$$

where C_0 and C_e are initial and equilibrium final concentrations (mg/L) of the metal solutions respectively. V (L) is the volume of metal solution and W (g) is the total mass of the used adsorbent.

To investigate the adsorption performance, adsorption isotherms for the individual adsorption of (Pb(II), Hg(II) and As(III)) were studied by contacting the optimum dose of adsorbent with different metals solutions at a different initial concentrations (25–250 mg/L).

The isotherms data were analyzed, fitted and plotted using Origin Pro 2016 Ver. 9.3.226 for different non-linear regression models shown in Table 1.

The mechanism of adsorption was studied by applying kinetic models using the optimized dose and pH for different time intervals (5, 10, 15, 20, 25, 30, 40, 60, 90, 120, and 150 min) and the used kinetic models are shown in Table 1

2.5. Desorption of metal ions and reusability of adsorbents and leaching studies

Metal-loaded MHAP samples (initial concentration of metal ions 10 mg/L, at room temperature) separated after the adsorption experiments were used in the desorption studies. Metal ions were eluted using ethylenediaminetetraacetic acid (EDTA 0.3 M).

After desorption, the composite was separated by filtration and metals concentration was measured then the adsorbent was rinsed with deionized water till the pH was neutral then dried and reconditioned for reuse in another run. The leaching potential of Fe was studied under different pHs (2, 4, 7 and 9) and different time intervals of 10, 30, 60, 120 min and 24 h.

3. Results and discussion

3.1. Characterization

The XRD pattern of the prepared magnetite, HAP and MHAP nanoparticle are shown in Fig. 1. The characteristic peaks of HA appear at 2θ of 29.1 and 31.8 that arising from calcium hydrogen phosphate. The characteristic peaks corresponding to the prepared magnetite have been observed at 2θ of 30.3, 35.6, 43.2, 53.5, 57 and 62.7. In the prepared composite, the diffraction peaks consist of both hydroxyapatite and magnetite nanoparticles revealing that hydroxyapatite structure was maintained even after the addition of magnetite nanoparticles with peaks appeared at 2θ values of 30.3 and 32.07.

Fig. 2 shows the FTIR spectra of the prepared HAP and MHAP nanocomposites. The bands at 3,423.99–3,770.15 cm^{-1} in the FTIR pattern of the is due to OH^- group which also found at 572.7 cm^{-1} . Peaks of the HAP functional groups of OH and PO_4 were found in the composite chart. The bands of PO_4^{3-} were detected at 1,046–1,428 and 572 [16]. A band of CO_3^{2-} was detected in the region around 1,428–1,633 cm^{-1} [17]. The strong band at 566.96 cm^{-1} in the composite is characteristic of Fe–O vibration of the magnetite nanoparticles. Other important characteristic peaks are observed at 2,347–363 cm^{-1} due to the presence of C–H groups.

The magnetic properties of the prepared magnetite and MHAP were studied using a vibrating sample magnetometer with a magnetic field application ranging from –20,000 to 20,000 G.

The magnetization curves are shown in Fig. 3 and they reveal the paramagnetic properties for the prepared magnetite and the composite. The saturation magnetization (M_s) value of the composite is 41.04 emu/g which is less than

Table 1
Kinetics and isothermal models (non-linear form)

	Non-linear form	Parameter
Kinetic models		
Pseudo-first-order	$q_t = q_e - (1 - e^{(-k_1 t)})$	k_1 (1/min) is the pseudo-first-order rate constant
Pseudo-second-order	$q_t = \frac{K_2 q_e^2 t}{1 + k_2 q_e t}$	k_2 (mg/g min) is the pseudo-second-order rate constant
Isotherm models		
Freundlich model	$q_e = K_F C_e^{1/n}$	K_F (L/g) Freundlich constant related to adsorption capacity; n Freundlich constant related to adsorption intensity;
Langmuir model	$q_e = q_m K_L \frac{C_e}{1 + K_L C_e}$	q_m (mg/g) maximum monolayer adsorption capacity; K_L (L/mg) Langmuir equilibrium constant.
Dubinin–Radushkevich (D–R) model	$q_e = q_s e^{(-K_{DR} \varepsilon^2)}$, $\varepsilon = RT \ln \left(1 + \frac{1}{C_e} \right)$ $E = \frac{1}{\sqrt{-2\beta}}$	b (mol^2/J^2) D–R constant; R (8.314 J/mol K) general gas constant; T (K) absolute temperature; E (kJ/mol) mean free energy.
Redlich–Peterson model	$q_e = \frac{K_{RP} C_e}{1 + a_{RP} C_e^g}$	K_{RP} (L/mg) is R–P constant related to the adsorption capacity; a_{RP} (L/mg) is a constant related to the affinity of the binding sites; g (g) is an exponent related to the adsorption intensity.

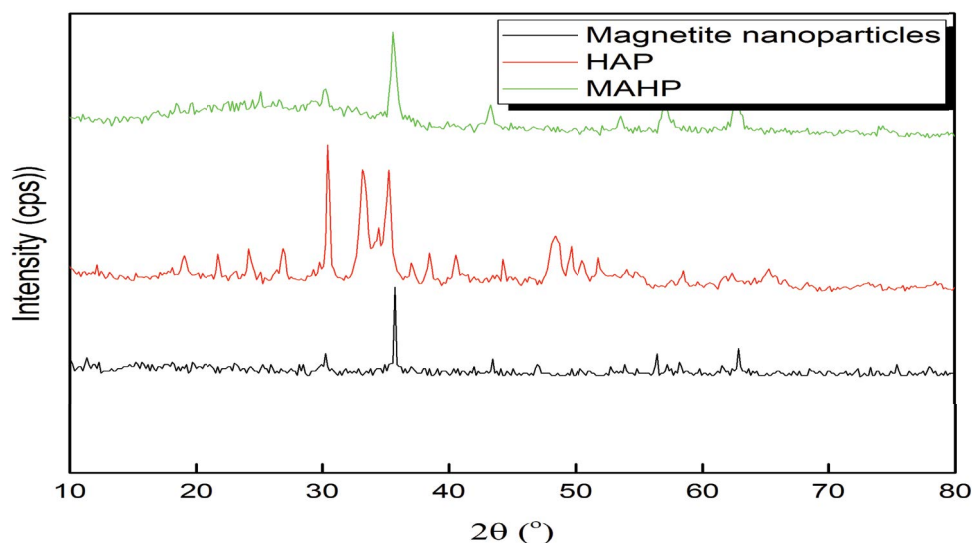


Fig. 1. XRD pattern of the prepared magnetite, HAP and MHAP nanoparticles.

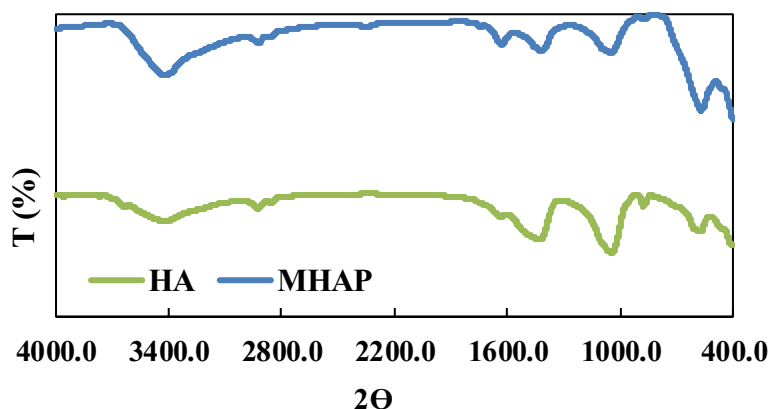


Fig. 2. FTIR spectra of the prepared HAP and MHAP nanocomposites.

that of the prepared magnetite nanoparticle (88.2 emu/g) and this maybe due to that the magnetic sites occupied by binding with HAP. MHAP can be easily attracted by an external magnetic field as previous studies have reported that 16.3 emu/g of saturation magnetization is enough for magnetic separations with a conventional magnet [18].

The typical TEM images of the prepared MHAP nanocomposites are shown in Fig. 4, where a cubic-shaped magnetite nanoparticle was found with size ranges between 8.9 and 35.4 nm.

The result of EDX spectra for the prepared MHAP showed the presence of Ca, P, O, and Fe and no other impurities were detected. EDX data. The analysis showed that the Ca/P ratio is 1.63 which is close to the stoichiometric ratio of 1.67. Furthermore, in a reasonable agreement with the obtained Ca/P, a ratio of 1.65 was found by ICP-OES analysis of the digested dissolved powders. The mass ratio of Fe/P is 1.1 which is in line with the calculated ratio for the preparation. The lead peak could be observed in lead-loaded MHAP which reveals the adsorption of lead ions on the nanocomposite surface. Moreover, calcium and phosphate

peaks were decreased in lead-loaded MHAP samples which might be due to the participation of lead ions adsorption.

The N_2 adsorption–desorption isotherm of the prepared HA, magnetite nanoparticles and MHAP is shown in Fig. 5. The isotherms of HA and MHAP showed type-IV, according to the classification of physisorption, with an H4 hysteresis loop, revealing the mesoporous structure and the amount of adsorption increased slowly at lower pressures. The isotherms of magnetite nanoparticles showed type-V with an H1 hysteresis loop, which can be caused by the weak adsorbent–adsorbate interactions. The Type H1 loop strengthens that materials exhibit a narrow range of uniform mesopores.

The specific surface area and total pore volume of the prepared composite are 42.7 m^2/g and 0.068 cm^3/g respectively. The mean pore size of the prepared composite is 6.4 nm which suggesting the presence of mesopores (2–50 nm). The prepared composite has a greater specific surface compared to the prepared magnetite and apatite which were 34 and 9.4 m^2/g respectively. The total pore volume of the prepared magnetite and apatite were 0.12 and

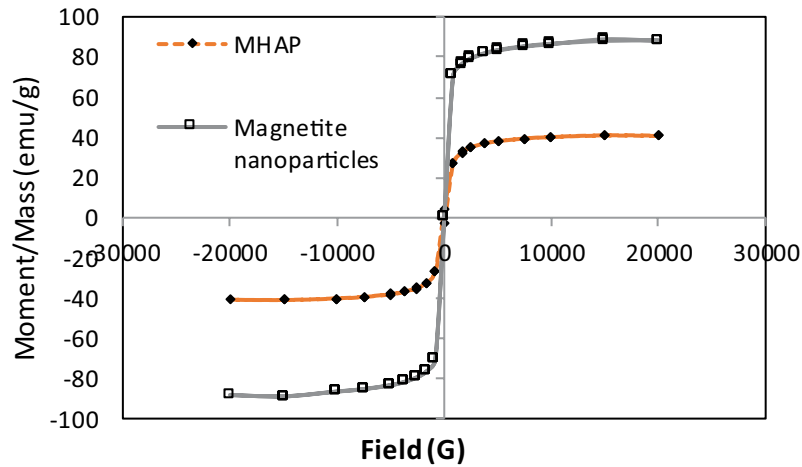


Fig. 3. The magnetization curves of the prepared magnetite and MHAP nanoparticles.

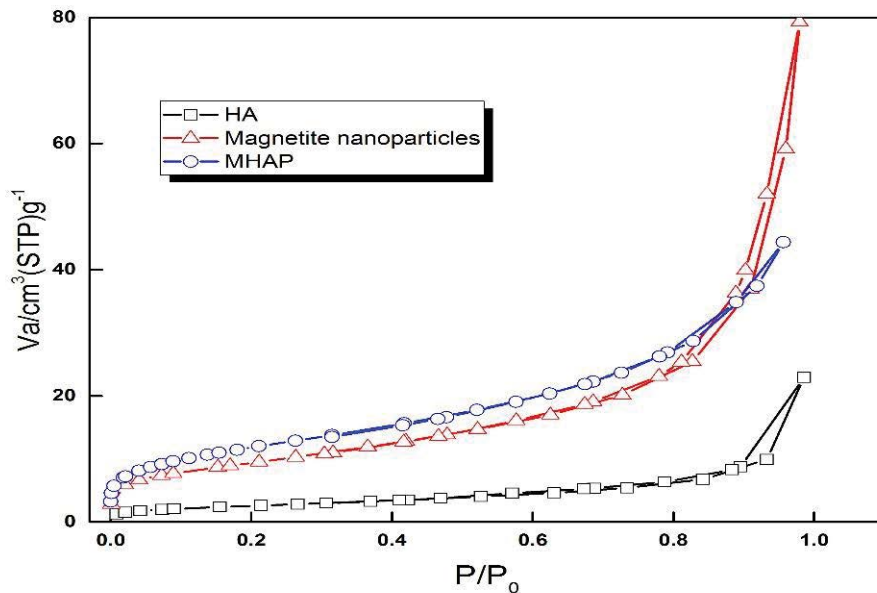


Fig. 5. N₂ adsorption–desorption isotherms of the prepared materials.

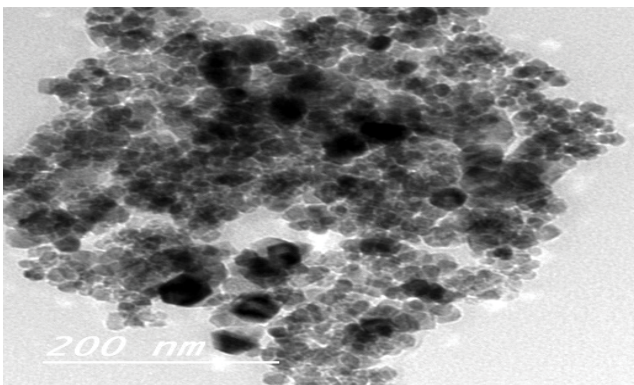


Fig. 4. TEM images of the prepared MHAP nanocomposites.

0.035 cm³/g respectively. The relative pressure (P/P_0) values were close to 1.0 indicating the mesoporous nature of the prepared composite. These results indicated that biogenic nHAP exhibited a higher surface area than that of the previously reported commercial nHAP (40.98 m²/g) [19].

3.2. Adsorption studies

The reaction between metal ions and the prepared composite was investigated by kinetics studies at different time intervals. First-order and second-order models (Table 1) are the extensively used kinetic equations for the sorption of a liquid–solid systems.

Table 2 shows the obtained parameters of equation models. The correlation coefficient (R^2) for the plot of the second-order model was higher than the first-order model and closer to 1. The values of the adsorption capacity (q_e)

were consistent with the experimental values which confirm its fitting to the kinetic data and suggesting that the rate-determining step occurs by chemisorption through exchange or sharing electrons between the adsorbent and adsorbate [20].

The removal of Pb(II), Hg(II) and As(III) ions by the prepared composite are shown in Fig. 6, Pb²⁺ ions removal showed a gradual increase with time and had the greatest removal percentage of 99% at 30 min then the adsorption reached equilibrium and adsorption slowed down as more atoms enter the adsorbent pores and reacting with the active sites.

The removal of Hg(II) and As(III) ions attained 80% and 66% at 60 and 120 min respectively. At higher concentrations of metal ions solutions, the adsorption decreases. Lead ions easily enter the pore sites and have a greater

Table 2
Parameters for kinetics and isotherm models fit

Metal	Pseudo-first-order			
	$q_{e,exp}$ (mg/g)	$q_{e,cal}$ (mg/g)	k_1	R^2
Pb(II)	9.9	9.53	0.57	0.06
Hg(II)	8.6	7.74	0.15	0.05
As(III)	7.2	6.50	0.21	0.06
	Pseudo-second-order			R^2
	$q_{e,cal}$ (mg/g)	k_2 (g/mg min)		
Pb(II)	9.94	0.22		0.98
Hg(II)	8.81	0.02		0.98
As(III)	7.23	0.04		0.98
Langmuir isotherm parameters				
	q_m (mg/g)	K_L (L/mg)	R^2	
Pb(II)	348.3	0.09	0.97	
Hg(II)	291.4	0.009	0.99	
As(III)	266.2	0.007	0.98	
Freundlich isotherm parameters				
	$1/n$	K_f (L/mg)	R^2	
Pb(II)	0.43	56	0.99	
Hg(II)	0.64	7.3	0.99	
As(III)	0.67	4.9	0.99	
D–R isotherm parameters				
	β (mol ² /g ²)	E (kJ/mol)	R^2	
Pb(II)	3.2×10^{-6}	11.2	0.90	
Hg(II)	9.9×10^{-5}	8.7	0.90	
As(III)	1.4×10^{-4}	8.1	0.90	
Redlich–Peterson parameters				
	K_R (L/mg)	a_R (L/mg)	g (g)	R^2
Pb(II)	96.6	1.1	0.67	0.99
Hg(II)	3.36	0.03	0.77	0.99
As(III)	5.21	0.50	0.44	0.98

affinity of the functional groups (OH⁻ and PO₄⁻³) comparing to Hg(II) and As(III) ions. The presence of Ca²⁺ in hydroxyapatite structure prefers to be incorporated with cations that have larger ionic radii. Therefore, precipitation of As(III) (0.058 nm) with Ca²⁺ would be less likely compared with the precipitation of larger cations Pb(II) (0.119 nm) and Hg(II) (0.109 nm).

EDX analysis of the composite loaded with Pb ions (highest removed metal) showed high P and Pb content and traces of Ca which reveals in the precipitation of Pb₁₀(PO₄)₆(OH)₂. The final (Ca + Pb)/P molar ratios obtained in the composite structure does not significantly vary from the initial Ca/P ratios in the prepared MHAP. Also, the ratio of (Ca + Pb)/Fe is similar to the initial Ca/Fe ratio as estimated by ICP-OES which indicates that the precipitation process occurring at the magnetic sphere surface.

The removal of different metals at different values of pH was determined. The adsorption of Pb(II) and Hg(II) increases with pH which may supports that the metal ions are adsorbed by an ion-exchange mechanism. When pH values increase in the range of 2–6 most of the metals exist as metal ions and the concentration of H⁺ ions will decrease.

Adsorption of Pb ions at pH values above 6 is due to the precipitation of non-soluble metal hydroxide MOH⁺ and M(OH)₂, so the experiments did not continue after pH 6 and the optimum pH was found to be 5.5 for Pb ions where the removal percentage recorded 99%.

At pH < 4, the predominant species of mercury ions are in Hg(II) forms, while mercury ions exist mainly in a neutral form Hg(OH)₂ at pH > 6 and between pH 4 to 6, Hg(OH)⁺ exists [21]. The optimum pH value was chosen as 5.5 for the further adsorption investigations where the removal percentage was 85%.

For As(III) ions, the removal increase at pH values range between 2–4 and the highest removal is 72% at pH 4. At higher pH values (pH > 4), As(III) may present as H₂AsO₃⁻ and HASO₃²⁻ anions which increasing the competition of hydroxyl ions for adsorption sites results in decreasing the removal.

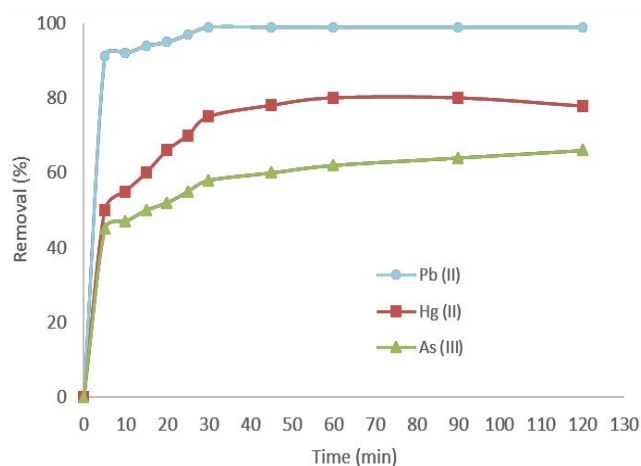


Fig. 6. Effect of time on of Pb(II) (pH, 5.5; dose, 1 g/L), Hg(II) (pH, 5.5; dose, 1 g/L; contact time) and As(II) (pH, 4; dose, 1 g/L) removal by the prepared composite.

The removal of metal ions increases with the adsorbent dose. The removal reaches 99% of Pb(II) ions at an adsorbent dosage of 0.5 g/L. Maximum removal of Hg²⁺ and As(III) reached 85% and 72% respectively using a dosage of 1 g/L.

Different isotherm models such as Langmuir, Freundlich, Dubinin–Radushkevich and Redlich–Peterson are applied to the experimental data to determine the adsorption capacity during equilibrium. Non-linear forms of isotherm models are shown in Table 1.

Models fitting is shown in Fig. 7 and the parameters of the equations are shown in Table 2. The experimental data were better fitted with the Langmuir model for Hg(II) where the calculated value of R^2 exhibited more close to 1 suggesting that the binding of mercury occurs by monolayer adsorption on the homogenous adsorbent surface.

The efficiency of the prepared composite has been compared with other reported adsorbents in Table 3 and as shown, the values of q_m for the prepared composites have higher values compared to the other magnetic and low-cost adsorbents.

In Freundlich adsorption isotherm applied for heterogeneous surfaces, the obtained $1/n$ values from applying Freundlich isotherm were higher than 0 but lower than 1 revealing that the adsorption is favorable. On the other hand, the adsorption is unfavorable when $1/n$ is higher than 1 [22]. The adsorption of Pb(II) and As(III) showed a higher value of R^2 when applying Freundlich adsorption isotherm assuming the multilayer adsorption.

The correlation coefficient for the Dubinin–Radushkevich isotherm, which is applied to express the energy distribution on a heterogeneous surface, is the lowest compared to the other isotherm models (Table 2).

The magnitudes of the mean adsorption energy (E), which gives information about adsorption type [23], were estimated to be 11.2, 8.7 and 8.1 kJ/mol for Pb(II), Hg(II) and As(III) respectively. Values of E that between 8 and 16 kJ/mol, revealing that the adsorption process proceeds by chemisorption through ion exchange reactions. On the other hand values of $E < 8$ kJ/mol, assumes that the adsorption has a physical nature [23].

The adsorption equilibrium that occurs in homogeneous or heterogeneous systems is represented by Redlich–Peterson isotherm model. At high concentrations with the exponent β tends to zero, the isotherm approaches the Freundlich isotherm model. While with lower concentrations at β values close to 1 the model approaches Langmuir isotherm conditions.

The highest value of g in Redlich–Peterson isotherm, as listed in Table 2, and that is the closest to 1 is that for Hg(II) adsorption, revealing the approaching to Langmuir form and the favorable adsorption [24].

3.3. Desorption of metal ions and reusability of adsorbents and leaching studies

The results of desorption studies showed that a great amount of metal ions desorbed using 0.3 M EDTA solution. An increase in desorption for Pb ions with a percentage of 99% was determined, followed by percentages of 97% and 95.5% for Hg(II) and As(III) respectively

By applying adsorption/desorption cycles, no significant loss in adsorption efficiency for the prepared composite in the four consecutive cycles, revealing the good reusability of the prepared adsorbent with long-term stability. No leaching of Fe ions was recorded during the desorption process.

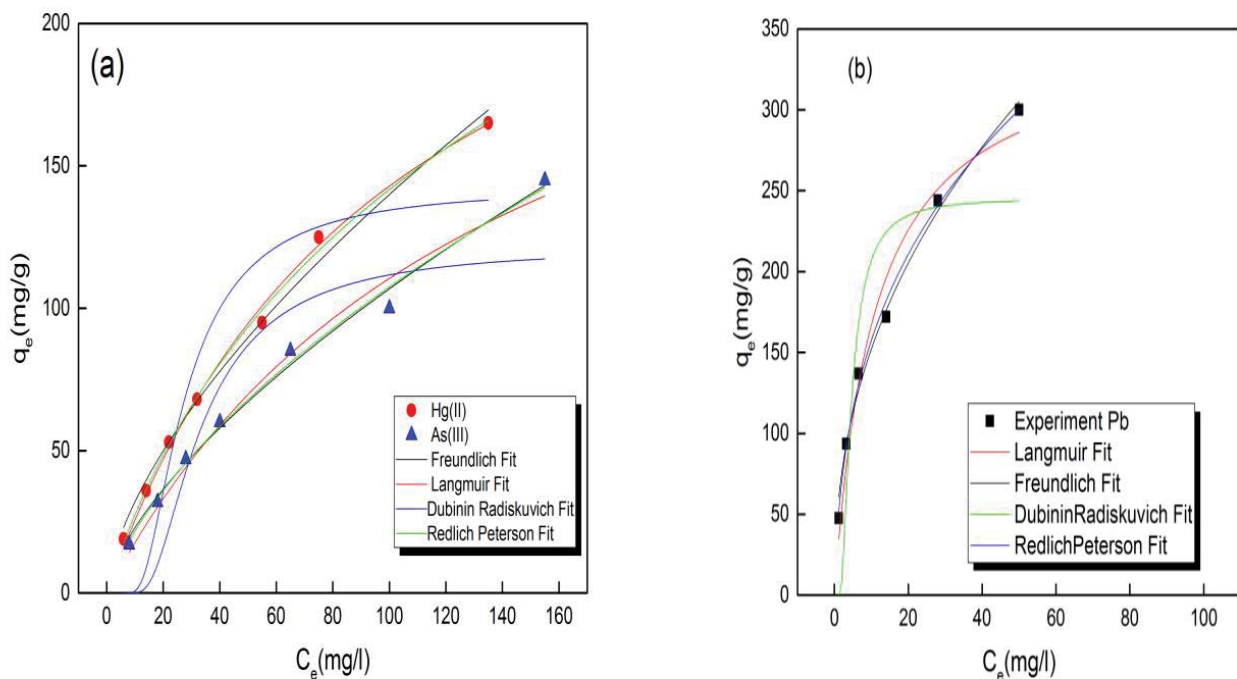


Fig. 7. Isotherms models pattern for the adsorption of (a) Hg(II) (pH, 5.5; dose, 1 g/L; contact time, 60 min) and As(II) (pH, 5.5; dose, 1 g/L; contact time, 120 min) and (b) Pb(II) (pH, 6; dose, 0.5 g/L; contact time, 30 min) on the prepared composite.

Table 3

Comparison of the adsorption capacities (q_m) of different composites for heavy metals

	Metal	q_m (mg/g)	Reference
Chicken feather	Pb(II)	1.1499	[25]
Etching iron oxide NPs	As(III)	42	[26]
Fe-Y materials (0.2 g/L)	As(III)	73	[27]
Hydroxyapatite from chicken bones	Pb(II)	105.26	[28]
Conjugate material	Pb(II)	214.15	[29]
Waterworks sludge	Pb(II)	20.409	[30]
Ti(IV) iodovanadate cation exchanger (TIV)	Hg(II)	21.32	[31]
Composite material (ligand immobilization onto the silica monolith)	Pb(II)	204.34	[32]
Magnetic hydroxyapatite nanocomposite (MHAP)	Pb(II)	348.3	This study
	Hg(II)	291.4	
	As(III)	266.2	

The leaching potential of Fe was studied under different pHs (pH 2, 7 and 10). Iron was leached to a small extent at pH 2 with a concentration of 0.01 mg/L. However, Fe concentrations in the leachate were found negligible at pH range 7 and 10.

4. Conclusions

The environmentally friendly recoverable magnetic hydroxyapatite composite (MHAP) was prepared using modified iron waste and eggshells. The prepared composite showed a high affinity for Pb(II), Hg(II) and As(III) ions and the adsorption was best fitted with a pseudo-second-order model. High values of maximum adsorption capacities for the tested metals, compared with other adsorbents, were obtained when applying the Langmuir isotherm model. EDTA solution was efficiently tested for metals desorption and the composite exhibited excellent reusability results.

Acknowledgments

Many thanks to the National Research Centre, Egypt, for providing facilities.

Funding

Not applicable.

Competing interests

The author declares that she has no competing interests.

References

- [1] S. Kavand, J.S. Lehman, S. Hashmi, L.E. Gibson, R.A. El-Azhary, Cutaneous manifestations of graft-versus-host disease: role of the dermatologist, *Int. J. Dermatol.*, 56 (2017) 131–140.
- [2] R. Dixit, D. Malaviya, K. Pandiyan, U.B. Singh, A. Sahu, R. Shukla, B.P. Singh, J.P. Rai, P.K. Sharma, H. Lade, Bioremediation of heavy metals from soil and aquatic environment: an overview of principles and criteria of fundamental processes, *Sustainability*, 7 (2015) 2189–2212.
- [3] C.-G. Lee, S. Lee, J.-A. Park, C. Park, S.J. Lee, S.-B. Kim, B. An, S.-T. Yun, S.-H. Lee, J.-W. Choi, Removal of copper, nickel and chromium mixtures from metal plating wastewater by adsorption with modified carbon foam, *Chemosphere*, 166 (2017) 203–211.
- [4] A. Masoumi, K. Hemmati, M. Ghaemy, Low-cost nanoparticles sorbent from modified rice husk and a copolymer for efficient removal of Pb(II) and crystal violet from water, *Chemosphere*, 146 (2016) 253–262.
- [5] B. Singha, N. Bar, S.K. Das, The use of artificial neural network (ANN) for modeling of Pb(II) adsorption in batch process, *J. Mol. Liq.*, 211 (2015) 228–232.
- [6] L. Zhi, W. Zuo, F. Chen, B. Wang, 3D MoS₂ composition aerogels as chemosensors and adsorbents for colorimetric detection and high-capacity adsorption of Hg²⁺, *ACS Sustainable Chem. Eng.*, 4 (2016) 3398–3408.
- [7] E.K. Faulconer, N.V.H. von Reitzenstein, D.W. Mazyck, Optimization of magnetic powdered activated carbon for aqueous Hg(II) removal and magnetic recovery, *J. Hazard. Mater.*, 199 (2012) 9–14.
- [8] L. Xu, X. Wu, S. Yuan, F. Xiao, M. Yang, Y. Jia, Speciation change and redistribution of arsenic in soil under anaerobic microbial activities, *J. Hazard. Mater.*, 301 (2016) 538–546.
- [9] D. Suteu, M. Badeanu, T. Malutan, A.-I. Chirculescu, Valorization of food wastes (orange seeds) as adsorbent for dye retention from aqueous medium, *Desal. Water Treat.*, 57 (2016) 29070–29081.
- [10] E.K. Radwan, S.T. El-Wakeel, T.A. Gad-Allah, Effects of activation conditions on the structural and adsorption characteristics of pinecones derived activated carbons, *J. Dispersion Sci. Technol.*, 40 (2019) 140–151.
- [11] A. Özer, Removal of Pb(II) ions from aqueous solutions by sulphuric acid-treated wheat bran, *J. Hazard. Mater.*, 141 (2007) 753–761.
- [12] K. Agrawal, G. Singh, D. Puri, S. Prakash, Synthesis and characterization of hydroxyapatite powder by sol-gel method for biomedical application, *J. Miner. Mater. Charact. Eng.*, 10 (2011) 727–734.
- [13] R.D. Ambashtha, M. Sillanpää, Water purification using magnetic assistance: a review, *J. Hazard. Mater.*, 180 (2010) 38–49.
- [14] O. Philippova, A. Barabanova, V. Molchanov, A. Khokhlov, Magnetic polymer beads: recent trends and developments in synthetic design and applications, *Eur. Polym. J.*, 47 (2011) 542–559.
- [15] P. Xu, G.M. Zeng, D.L. Huang, C.L. Feng, S. Hu, M.H. Zhao, C. Lai, Z. Wei, C. Huang, G.X. Xie, Use of iron oxide nanomaterials in wastewater treatment: a review, *Sci. Total Environ.*, 424 (2012) 1–10.
- [16] G. Kousalya, M.R. Gandhi, C.S. Sundaram, S. Meenakshi, Synthesis of nano-hydroxyapatite chitin/chitosan hybrid biocomposites for the removal of Fe(III), *Carbohydr. Polym.*, 82 (2010) 594–599.

- [17] C. Qi, Q.-L. Tang, Y.-J. Zhu, X.-Y. Zhao, F. Chen, Microwave-assisted hydrothermal rapid synthesis of hydroxyapatite nanowires using adenosine 5'-triphosphate disodium salt as phosphorus source, *Mater. Lett.*, 85 (2012) 71–73.
- [18] Z. Ma, Y. Guan, H. Liu, Synthesis and characterization of micron-sized monodisperse superparamagnetic polymer particles with amino groups, *J. Polym. Sci., Part A: Polym. Chem.*, 43 (2005) 3433–3439.
- [19] A. Ramdani, Z. Taleb, A. Guendouzi, A. Kadeche, H. Herbache, A. Mostefai, S. Taleb, A. Deratani, Mechanism study of metal ion adsorption on porous hydroxyapatite: experiments and modeling, *Can. J. Chem.*, 98 (2020) 79–89.
- [20] H. Ys, G. Mckay, H. Ys, G. Mckay, Pseudo-second-order model for sorption processes, *Process Biochem.*, 34 (1999) 451–465.
- [21] R. Das, S. Giri, A.M. Muliwa, A. Maity, High-performance Hg(II) removal using thiol-functionalized polypyrrole (PPy/MAA) composite and effective catalytic activity of Hg(II)-adsorbed waste material, *ACS Sustainable Chem. Eng.*, 5 (2017) 7524–7536.
- [22] M.H. Stietiya, J.J. Wang, Zinc and cadmium adsorption to aluminum oxide nanoparticles affected by naturally occurring ligands, *J. Environ. Qual.*, 43 (2014) 498–506.
- [23] A. Dada, A. Olalekan, A. Olatunya, O. Dada, Langmuir, Freundlich, Temkin and Dubinin–Radushkevich isotherms studies of equilibrium sorption of Zn²⁺ onto phosphoric acid modified rice husk, *IOSR J. Appl. Chem.*, 3 (2012) 38–45.
- [24] K.V. Kumar, S. Sivanesan, Equilibrium data, isotherm parameters and process design for partial and complete isotherm of methylene blue onto activated carbon, *J. Hazard. Mater.*, 134 (2006) 237–244.
- [25] N. Umedum, C. Anarado, A. Eboatu, Chicken feather as sequestrant for lead ions in aqueous solution, *Int. J. Modern Anal. Sep. Sci.*, 3 (2014) 51–66.
- [26] W. Cheng, W. Zhang, L. Hu, W. Ding, F. Wu, J. Li, Etching synthesis of iron oxide nanoparticles for adsorption of arsenic from water, *RSC Adv.*, 6 (2016) 15900–15910.
- [27] C. Qin, L. Liu, Y. Han, C. Chen, Y. Lan, Mesoporous magnetic ferrum-yttrium binary oxide: a novel adsorbent for efficient arsenic removal from aqueous solution, *Water, Air, Soil Pollut.*, 227 (2016) 337, doi: 10.1007/s11270-016-3032-7.
- [28] A. Vahdat, B. Ghasemi, M. Yousefpour, Synthesis of hydroxyapatite and hydroxyapatite/Fe₃O₄ nanocomposite for removal of heavy metals, *Environ. Nanotechnol. Monit. Manage.*, 12 (2019) 100233, doi: 10.1016/j.enmm.2019.100233.
- [29] M.R. Awual, M.M. Hasan, A ligand based innovative composite material for selective lead(II) capturing from wastewater, *J. Mol. Liq.*, 294 (2019) 111679, doi: 10.1016/j.molliq.2019.111679.
- [30] A.A. Faisal, S.F. Al-Wakeel, H.A. Assi, L.A. Najji, Mu. Naushad, Waterworks sludge-filter sand permeable reactive barrier for removal of toxic lead ions from contaminated groundwater, *J. Water Process Eng.*, 33 (2020) 101112, doi: 10.1016/j.jwpe.2019.101112.
- [31] Mu. Naushad, Z. AlOthman, M.R. Awual, M.M. Alam, G. Eldesoky, Adsorption kinetics, isotherms, and thermodynamic studies for the adsorption of Pb²⁺ and Hg²⁺ metal ions from aqueous medium using Ti(IV) iodovanadate cation exchanger, *Ionics*, 21 (2015) 2237–2245.
- [32] M.R. Awual, Innovative composite material for efficient and highly selective Pb(II) ion capturing from wastewater, *J. Mol. Liq.*, 284 (2019) 502–510.